Effects of Diverging and Converging Roughness on Turbulent Boundary Layers

B. Nugroho[1], N. Hutchins[1] and J. P. Monty[1]

[1]Department of Mechanical Engineering
The University of Melbourne, Victoria 3010, Australia

Abstract

This paper describes a parametric study of the development of zero pressure gradient turbulent boundary layer over diverging and converging *riblet-type* surface roughness geometries. The current study is an expansion to the preliminary investigation by Nugroho *et al* (10), where this type of surface roughness is used to induce large-scale counter-rotating flows and causes a high degree of three dimensionality over the spanwise wavelength of the surface roughness pattern. Previous data reveals that the secondary flows generated by the surface roughness are able to capture and lock-in the largest-scale motions (superstructures) of the flow, despite the fact that the riblet height is one hundred times smaller than the boundary layer thickness. Here we extend this work to include different riblet yaw angles α and viscous-scaled riblet height h^+. It was found that as α or h^+ decreases, the effect of surface roughness becomes less prominent on the secondary flow.

Introduction

Recent studies on wall bounded flows at high Reynolds number have revealed the importance of large-scale motions (LSM) scaling with boundary layer thickness, δ, e.g Kim and Adrian (6) and Balakumar and Adrian (1). LSMs are believed to be originated from hairpin vortices which move coherently in packets, have streamwise length of $2\delta - 3\delta$, and spanwise length of $1\delta - 1.5\delta$ (Kovasznay *et al* (8)). Further studies by Kim and Adrian (6) in wall-bounded flows with internal geometries have shown that there are even longer motions residing in the logarithmic region, which they termed as very large-scale motions (VLSMs). Evidence of VLSMs is found in the form of peak at long wavelength in the pre-multiplied spectra of streamwise turbulent fluctuations u. These type of motions are not believed to be a new type of eddy, instead it is presumed to result from the coherence in the hairpin packets pattern (Kim and Adrian (6)). Similar features have been reported by Hutchins and Marusic (4), where they found highly energetic fluctuations in the logarithmic region of the turbulent boundary layer. These features have very long meandering streamwise negative velocity fluctuations (instantaneous length 15δ - 20δ), flanked by positive velocity fluctuations on either side . Hutchins and Marusic (4) refer these very large features as 'superstructures'. They went further to say that superstructures leave footprint at the wall, resulting in significant contribution towards turbulent fluctuations and Reynolds stress production. It is believed that by disturbing these VLSMs and superstructures, an effective flow control or drag reduction mechanism may be achievable.

To date, there have been few studies on manipulating VLSMs or superstructures. One particular way is to employ ordered surface roughness, and in our case, we concentrate on riblet-type roughness. Riblets are a series of very small continuous grooves that can be used to cover the aerodynamic surfaces of vehicles. Highly ordered riblet-type surface roughness has attracted plenty of attention in the last three decades due to its ability to reduce skin friction drag (Bechert *et al* (3)). Investigations by Bechert and Bartenwerfer (2) have revealed that these small riblets are damping the cross-flow velocity fluctuations near the
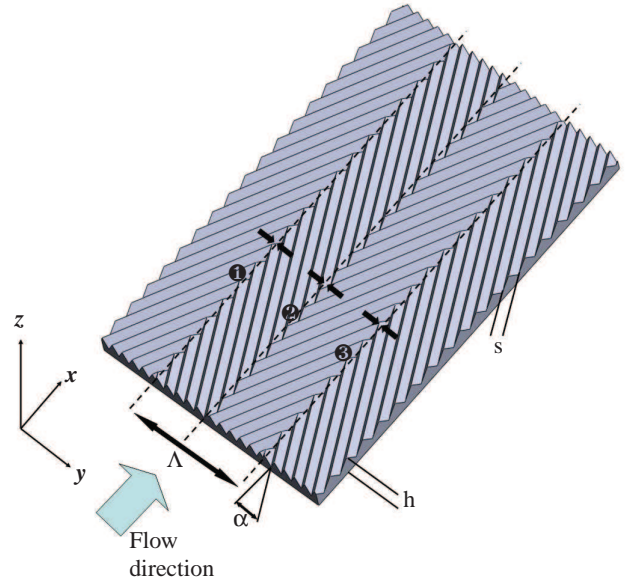

Figure 1: Schematic diagram of converging / diverging riblet pattern, showing regions of converging (regions ① and ③) and diverging (region ②) spanwise flow.

wall, resulting in the skin friction drag reduction. Although riblets have been proven to be an effective method for turbulent drag reduction in their standard form, they are believed to control the near-wall small scale coherent structures. There are no investigations that utilize the riblets in an attempt to control VLSMs or superstructures. Work by Koeltzsch *et al* (7) have shown that by aligning the riblets in diverging-converging configurations within a pipe flow, these surfaces can impose a large-scale spanwise modification to the boundary layer characteristics. Nugroho *et al* (10) has performed similar experiments for flat plate boundary layer and showed that the diverging-converging surface roughness is able to capture and lock-in the largest-scale motions in the flow. Based on these reports it is only natural to broaden the findings further by probing into different riblet parameters. The principal aim of this investigation is to expand the previous experiments by Nugroho *et al* (10), by considering two different parameters: riblet yaw angle, α, and viscous-scaled riblet height, h^+.

Surface Roughness Manufacturing

A schematic diagram of the diverging-converging riblet and key dimensions are shown in Figure 1. A master tile made of acetal copolymer has been cut using a high precision three axis CNC machine *CNC-Technik HEIZ S-1000* to form the diverging-converging template. The cutter used in this manufacturing process has a 60° tip, resulting in a riblet cut with a spacing of $s = 0.675$ mm and height $h = 0.5$ mm, leading to h/s ratio of 0.74. The diverging-converging angle of the riblet with respect to the mean flow, α, is set at 10°. This angle is chosen to be less aggresive than the 30° and 45° used by Nugroho *et al* (10) and

Surface		U_∞ (m/s)	h^+	s^+	δ_{98} (m)	$Re_{\tau s}$
smooth		10	-	-	0.0520	1300
div	②	10	13	18	0.0525	1300
con	①③	10	13	18	0.0580	1300
smooth		20	-	-	0.0519	2300
div	②	20	24	32	0.0526	2300
con	①③	20	24	32	0.0706	2300

Table 1: Experimental parameters for smooth, diverging, and converging surface.

Koeltzsch *et al* (7) respectively. The width of each diverging and converging region is 0.074 m, resulting in a repeating spanwise wavelength $\Lambda = 0.148$ m. The master tile has dimensions 0.515×0.296 m, contains two strips at $+10^o$ and two strips at -10°. Apart from α, all other physical parameters of this surface roughness are identical to thoses used by Nugroho *et al* (10). A mold of this master tile is then produced from silicone rubber and used to cast multiple copies of the pattern, that are used to cover the test surface in the facility.

Experimental set up and parameters

The experiments are performed in an open-return blower wind tunnel located in the Walter Basset Laboratory at The University of Melbourne. The wind tunnel has a cross-sectional area of 0.94×0.375 m and a 6.7 m long working section. This facility has a fully adjustable roof to enable accurate pressure gradient adjustment. In this experiment, the tunnel is set at zero pressure gradient. All measurements are made 4 m downstream of the inlet. The wind tunnel is operated at two free stream velocities $U_\infty = 10$ m/s and $U_\infty = 20$ m/s. For a hydronomically smooth wall, the Reynolds numbers are $Re_{\tau s} = 1300$ and $Re_{\tau s} = 2300$ respectively ($Re_{\tau s} = \delta_{98s} U_{\tau s}/\nu$, δ_{98s} is boundary layer thickness based on 98% of free stream velocity over smooth wall, ν is kinematic viscosity, and $U_{\tau s}$ is smooth wall friction velocity). The two sets of free stream velocities correspond to $h^+ = 13$ and $h^+ = 24$ respectively for the riblet surface, where $h^+ = hU_{\tau s}/\nu$.

All experiments are carried out with a single hot-wire probe operated in constant temperature using an in-house Melbourne University Constant Temperature Anemometer (MUCTA), with an overheat ratio of 1.8. A boundary layer type probe body geometry (*Dantec 55P15*) with prong spacings of 3 mm is used to hold the sensor element. The wire is a 5μm diameter platinum filament with an etched length of approximately 1 mm, resulting in length-to-diameter (l/d) ratio of 200. The l/d ratio is set to exceed 200 to minimize attenuation due to end conduction. The viscous scaled length l^+ of the hot wires for $U_{\tau s} = 1300$ and $U_{\tau s} = 2300$ is 26 and 47 respectively. These wires will suffer from some attenuation due to insufficient spatial resolution (Ligrani and Bradshaw (9) and Hutchins *et al* (5)). However, since these measurements are made for comparative purposes between smooth wall and riblets covered wall, the attenuation is deemed acceptable. For each Reynolds number, measurements are performed over smooth surfaces, and also over the diverging and converging regions of the riblet surfaces.

Results

Table 1 lists the boundary layer parameters for the smooth wall, and above the diverging region, and converging region for both sets of free stream velocity. Here U_∞ is free stream velocity, h^+ is viscous-scaled riblet height, s^+ is viscous-scaled riblet spacing, δ_{98} is boundary layer thickness based on 98% of free stream velocity, and $Re_{\tau s}$ is Reynolds number based on hydronomically smooth wall. From the table it is clear that the riblets have a significant effect on the boundary layer thickness. At
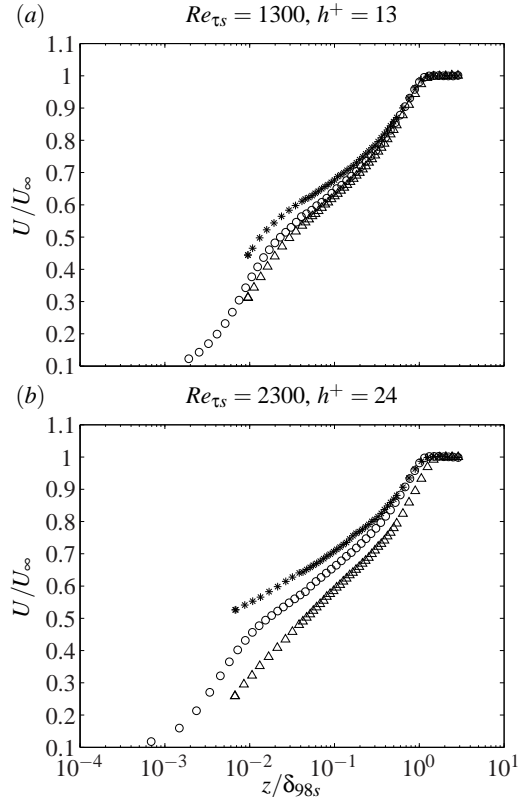

Figure 2: Mean velocity profile for $Re_{\tau s} = 1300$ (a) and $Re_{\tau s} = 2300$ (b) over the diverging ($*$) and converging ($\triangle$) regions of the rough surface, and for the smooth wall case ($\circ$). Velocity is non-dimensionalised using free stream velocity U_∞ and distance from wall is non-dimensionlised using boundary layer thickness over the smooth wall δ_{98s}

$h^+ = 13$, the boundary layer thickness over converging region is around 10% thicker than over the smooth wall. As h^+ increases, the differences in δ_{98} between the smooth wall and the converging region increases: for $h^+ = 24$ the difference is around 27%. Interestingly, the differences in δ_{98} between the smooth wall and the diverging region are quite marginal for both $Re_{\tau s}$ cases (approximately 1%). It appears that $\alpha = 10^o$ is not an aggressive enough angle to affect the boundary layer thickness over the diverging region. This result is in contrast to previous experiment by Nugroho *et al* (10), for $\alpha = 30^o$, where the riblet yaw angle is strong enough to modify the boundary layer thickness for flows over the diverging and converging region cases.

Figure 2(a & b) show the mean velocity profiles for the smooth wall case, and over the diverging and converging regions at the two h^+ conditions. The velocity axis is made non-dimensional by the freestream velocity, and the wall-normal distance is non-dimensionalised using boundary layer thickness over the smooth wall δ_{98s}. From the figure it is obvious that the local mean velocity over the diverging region is higher than that over the converging region. The differences in local velocities are even more pronounced at higher h^+ (figure 2b). Those differences contribute towards the changes in boundary layer thickness δ_{98}. As the local velocity decreases over the converging region, the boundary layer thickens, while the opposite happens over the diverging region. The results strongly suggest that the converging pattern of the riblets are forcing the low-speed fluid near the wall to move vertically away from the wall, resulting in lowered local streamwise velocities in this region. Conversely, the diverging pattern of the riblets are sweeping the high-speed fluid towards the wall, causing higher local streamwise veloci-
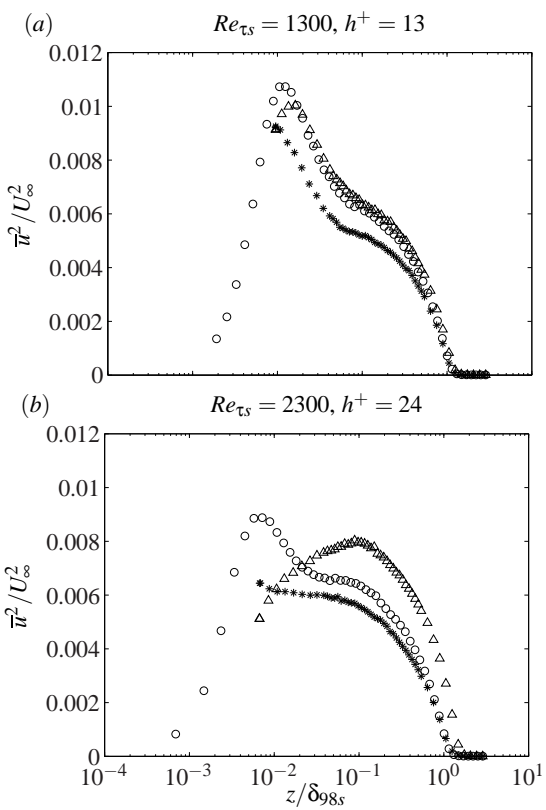
(a) $Re_{\tau s} = 1300$, $h^+ = 13$

(b) $Re_{\tau s} = 2300$, $h^+ = 24$

Figure 3: Turbulence Intensity for $Re_{\tau s} = 1300$ (a) and $Re_{\tau s} = 2300$ (b) over the diverging ($*$) and converging (Δ) regions of the rough surface, and for the smooth wall case ($\circ$). Turbulence intensity is non-dimensionalised using free stream velocity U_∞ and distance from wall is non-dimensionlised using boundary layer thickness over the smooth wall δ_{98s}
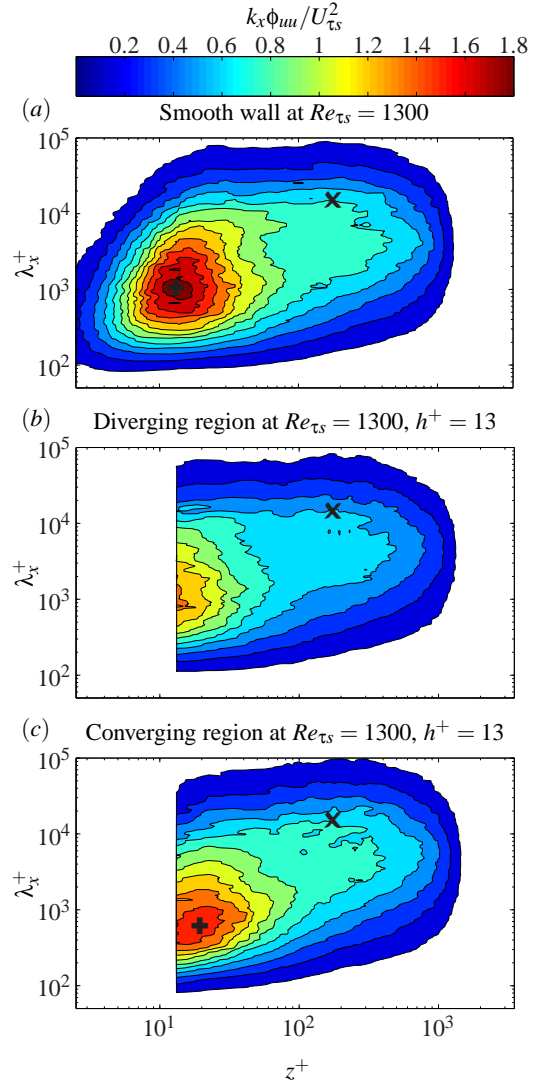

Figure 4: Contours of pre-multiplied streamwise energy spectra $k_x \phi_{uu}/U_{\tau s}^2$, where k_x is streamwise wavenumber and ϕ_{uu} is the energy spectra of streamwise velocity fluctuations. The pre-multiplied spectra is plotted as a function of wall-normal position z^+ and energetic streamwise length-scale λ_x^+. Plots are shown for the smooth wall case (a) and above the diverging (b) and converging (c) regions at $Re_{\tau s} = 1300$

ties. It is extraordinary that a surface pattern with such a small riblet height (h/$\delta_{98s} = 0.01$) is able to produce spanwise variation in boundary layer and local streamwise velocity. The flow behavior seems to suggest that there are large-scale counter rotating vortices existing above the surface roughness. The modifications to the mean velocity profile are in general less severe compared to the previous work by Nugroho *et al* (10). As α decreases, the effectiveness of the diverging and converging riblets to impose large-scale secondary flows diminishes.

Streamwise turbulent intensity profiles in figure 3(a & b) show that for both h^+, the intensities over the diverging region decreases. For the converging region, the turbulent intensity for $h^+ = 13$ is slightly lower than the smooth wall case, and the peak seems shifted away from the wall. In the case of $h^+ = 24$ the turbulent intensity peak is clearly shifted towards the logarithmic region, it climbs beyond the smooth wall case at $z/\delta_{98s} = 0.02$ and reaches its peak at $z/\delta_{98s} = 0.1$. These phenomena suggest that the vertical motion over the converging region redistributes the near-wall turbulence intensity (which is generally high) into the outer regions of the boundary layer. Conversely, the low turbulence intensity in the outer region above the diverging pattern is swept towards the wall, resulting in a lower localised turbulent intensity.

Figures 4 and 5 show pre-multiplied energy spectra maps for the smooth wall, and diverging and converging region for both Reynolds numbers. These color contours show the pre-multiplied streamwise spectra $k_x \phi_{uu}/U_{\tau s}^2$ as a function of wall normal position, z^+, where $z^+ = zU_{\tau s}/\nu$, and streamwise length-scale, λ_x^+, where $\lambda^+ = \lambda U_{\tau s}/\nu$. The energy spectras are

normalised by the smooth wall friction velocity, $U_{\tau s}$, since it is not possible at this time to obtain $U_{\tau s}$ over the rough surface. The use of the modified Clauser technique to obtain U_τ over the rough surface is questionable due to the strong changes in wake strength. In standard zero-pressure-gradient wall bounded flow it is observed that there are two local peaks on the spectral surfaces. The first peak, termed as *inner peak* (marked by symbol +) is located at $z^+ = 15$ and $\lambda_x^+ = 1000$ (Hutchins and Marusic (4)). This peak exists due to near-wall cycle of streaks and quasi-streamwise vortices (Schoppa and Hussain (11)). The second peak which termed as *outer peak*, (marked by symbol ×) is located at $z/\delta = 0.06$ and $\lambda_x/\delta = 6$, and exists due to superstructure type events (Hutchins and Marusic (4)). For canonical smooth wall turbulent boundary layer, this outer peak increases in magnitude as Reynolds number increases. Figure 4a and Figure 5a show evidence of how the outer peak grows with Reynolds number. For the case of the diverging region at $Re_{\tau s} = 1300$ (Figure 4b), the surface roughness forces the inner peak spectra to move closer to the wall, and reduces the overall energy spectra magnitude. At $Re_{\tau s} = 2300$ (Figure 5b) the diverging region also exhibits an inner peak spectra that is pushed
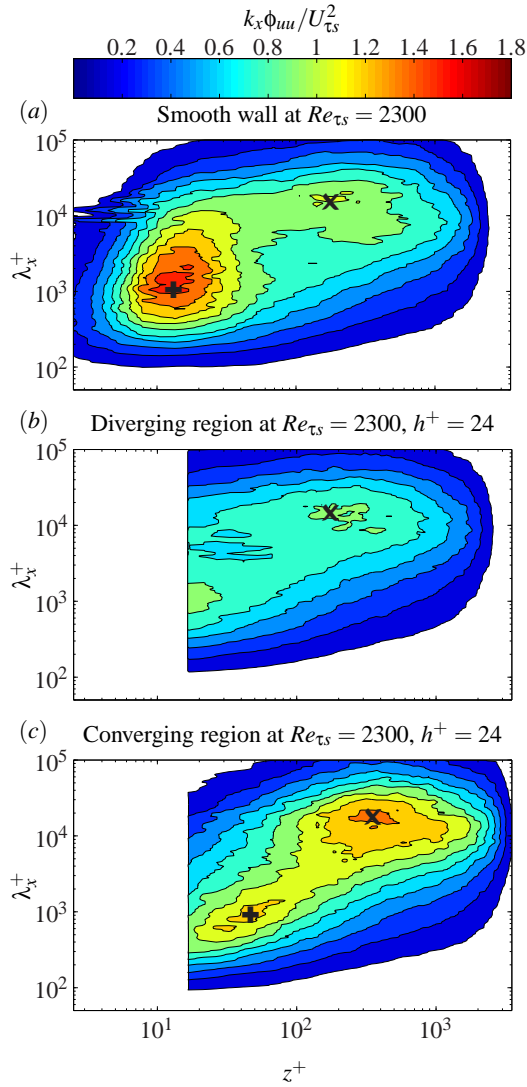
Figure 5: Contours of pre-multiplied streamwise energy spectra for the smooth wall case (a) and above the diverging (b) and converging (c) regions at $Re_{\tau s} = 2300$.

even closer towards the wall and the overall energy spectra magnitude is lowered. From figure 5b it is also noted that there is an outer peak located at $z^+ \approx 250, \lambda_x^+ \approx 15000$ although it is lower in magnitude than the smooth wall. Over the converging region at lower h^+ (Figure 4c), the inner peak is slightly shifted to $z^+ \approx 20$, $\lambda_x^+ \approx 500$ from the smooth wall case at $z^+ \approx 15$, $\lambda_x^+ \approx 1000$. For $h^+ = 24$ the converging region on Figure 5c clearly shows a highly energetic outer peak located at $z^+ \approx 500$, $\lambda^+ \approx 20000$. Thus It appears, that for the $h^+ = 24$ case there is increased large-scale energy over the diverging region and decreased large-scale energy over the diverging region, suggesting that the superstructure type events have been captured and locked in location over the converging region. All of the spectra plots confirm that as h^+ increases, the effectiveness of the surface roughness in imposing large-scale modifications also increases.

Summary and Conclusions

A parametric study of zero pressure gradient turbulent boundary layer over a diverging and converging riblet-type surface roughness has been conducted. The surface roughness imposes secondary flows causing large-scale spanwise modifications to the boundary layers thickness, mean velocity, and turbulent intensity. The data shows that the local mean velocity above the converging region decreases, while the turbulent intensity in-

creases. The opposite phenomena occurs over the diverging region. Based on these findings, it is proposed that this type of surface roughness is generating large-scale counter rotating roll-mode inside the turbulent boundary layer, with an upward flow direction occuring above the converging region, and downward flow direction above the diverging region. The boundary layer thickness, δ_{98}, in the converging case for both sets of Reynolds number, $Re_{\tau s}$, show that they are thicker than the smooth wall case. However, there is not much difference in boundary layer thickness δ_{98} between the diverging and the smooth wall case for both Reynolds number cases. It appears that a larger diverging-converging angle α is required to affect the boundary layer thickness over the diverging region. As h^+ increases, the strength of the secondary flow also increases, resulting in dramatic large-scale modifications. Further analysis on the pre-multiplied energy spectra suggests that the surface roughness is able to lock the largest-scale motions of the turbulent flow in place over the converging regions. Further experiments (either by PIV or rake type measurements) are required to confirm this.

*

References

[1] Balakumar.B.J and Adrian.R.J, Large- and very-large-scale motions in channel and boundary-layer flows, *Phil. Trans. R.Soc. Lond. A*, **365**, 2007, 665–681.

[2] Bechert.D.W and Bartenwerfer.M, The viscous flow on surfaces with longitudinal ribs, *J. Fluid Mech*, **206**, 1989, 105–129.

[3] Bechert.D.W, Bruse.M, Hage.W, Hoeven.J.G.Th, V. D. and Hoppe.G, Experiments on drag-reducing surfaces and their optimisation with an adjustable geometry, *J. Fluid Mech*, **338**, 1997, 59–87.

[4] Hutchins.N and Marusic.I, Evidence of very long meandering features in the logarithmic region of turbulent boundary layers, *J. Fluid Mech*, **579**, 2007, 1–28.

[5] Hutchins.N, Nickles.T.B, Marusic.I and Chong.M.S, Hot-wire spatial resolution issues in wall bounded turbulence, *J. Fluid Mech*, **635**, 2009, 103–136.

[6] Kim.K.C and Adrian.R.J, Very large-scale motion in the outer layer, *J. Fluid Mech*, **11**, 1999, 417–422.

[7] Koeltzsch.K, Dinkelacker.A and Grundmann.R., Flow over convergent and divergent wall riblets, *Exp. Fluids*, **33**, 1967, 346–350.

[8] Kovasznay.L.S.G, Kibens.V and Blackwelder.R.F, Large-scale motion in the intermittent region of a turbulent boundary layer, *J. Fluid Mech*, **41**, 1970, 283–326.

[9] Ligrani.P.M and Bradshaw.P, Spatial resolution and measurement of turbulence in the viscous sublayer using sub-miniature hot-wires probes, *Exp. Fluids*, **5**, 1987, 407–417.

[10] Nugroho.B, Kulandaivelu.V, Harun.Z, Hutchins.N and Monty.J.P, An investigation into the effects of highly directional surface roughness on turbulent boundary layers, *17th Australasian Fluid Mechanics Conference*.

[11] Schoppa, W. and Hussain.F, Coherent structure generation in near-wall turbulence, *J. Fluid Mech*, **453**, 2002, 57–108.